This is the post-print of an article published in
Journal of Energy Storage, Volume 13, October 2017, Pages 244–254

Dynamic mismatch losses of grid-connected PV-battery systems in residential buildings

Johannes Weniger[1], Tjarko Tjaden, Joseph Bergner, Volker Quaschning

HTW Berlin – University of Applied Sciences,
Department 1 – Energy and Information,
D-12459 Berlin, Germany

Abstract

Battery energy storage devices coupled with photovoltaic (PV) systems have to react to the fluctuating nature of the PV output and electrical demand in residential buildings. However, the charging and discharging power cannot be adjusted to the power fluctuations without any time delay so that an inherent temporal mismatch between the battery power and the residual power (PV output minus load) occurs under dynamic conditions. This paper presents a simulation study analyzing the response time-induced mismatch losses of grid-connected PV-battery systems. Firstly, the response time issue is analyzed theoretically to reveal how the energy flows between the household and the grid are changed due to the delayed battery response. Then, measurements are presented to show the dynamic behavior of two different PV-battery systems. The experimental results reveal settling times of up to 7 s to reach the steady state after an abrupt step change in the load demand. Thirdly, simulations of an AC-coupled PV-battery system are carried out with a time step size of 1 s. A sensitivity analysis is conducted to identify the impact of the dynamic response on the annual amount of energy exchanged with the grid. It is found that longer response times are accomplished by an increase in the grid feed-in and grid supply as well. Consequently, a slow-reacting battery system diminishes the economic benefit for the owner of the PV-battery system. In order to improve the transparency from the end-customer´s point of view, response time-related specifications should be stated in the data sheets of the products in the future.

Keywords: Electric energy storage; Battery storage; PV-battery system; Response behavior; Control system

[1] Corresponding author. E-mail address: pvstorage@htw-berlin.de.

1 Introduction

The cost situation of photovoltaic (PV) generated electricity and grid electricity has been changed drastically in many European countries over the recent years [1]. The levelized cost of PV electricity undercut the retail electricity price in Germany around 2011 [2]. Consequently, it is becoming more attractive to utilize the PV energy on-site instead of feeding it into the grid, especially at the domestic level. Thus, PV energy is used primarily to cover the electrical load in a household to substitute electricity purchased from the grid. However, the share of the annual PV generation that is consumed directly by the home owners is limited due to the low temporal matching capability between the load demand and on-site PV generation in both the diurnal and seasonal course. Different options exist to increase the PV self-consumption, where the two major ones are active load shifting by means of load management and energy storage with batteries [3]. Load management aims at shifting deferrable loads to periods of surplus PV generation so that the amount of energy drawn from the grid is reduced. The conjunction of PV systems with batteries enables an additional increase of the on-site self-supply of domestic buildings [4]. For this purpose, PV surpluses during the day are stored to supply the electrical load in the evening and at night-time. Today, there are numerous PV-battery systems for the application in residential buildings available on the market. Such a PV-battery system usually consists of a common PV system composed of several modules and one or more power inverters, a storage device with a battery and a control unit. The battery can either be linked to the AC- or DC-side of the PV inverter. AC-coupled battery storage systems are equipped with bidirectional battery inverters, while unidirectional inverters are usually integrated into DC-coupled systems. However, there are also DC-coupled systems with bidirectional inverters which can be charged from the AC-side [5].

In order to regulate the power flows in buildings equipped with PV-battery systems, different control strategies can be implemented [6–8]. Since the main objective is to minimize the energy exchanged with the grid; the battery power is regulated with respect to the active power flows measured at the point of common coupling. In this way, the power absorbed or provided by the battery system is adjusted according to the actual power balance of the household affected by the on-site generation and load demand. By doing so, the battery power must follow the fluctuating characteristic of the generation and load curve. On the one hand, shadows induced by moving clouds are the major reason for abrupt changes in the PV power output [9]. The PV output fluctuates rapidly in time scales ranging from a few seconds to several minutes during scattered cloudy days [10]. On the other hand, switching electrical devices causes peaks and steep ramps in the demand curve of single-family households in small time scales. As a result, the battery power control unit has to react to short-term power fluctuations induced by both the PV output and load demand.

To ensure control stability and due to the general fact that information acquisition and processing procedures commonly have an inherent time delay, the battery power control is subjected to response time issues. Therefore, a short period of time passes before the battery power is adjusted properly in accordance with the observed residual

PV power or residual load demand. In other words, the battery charging and discharging power cannot perfectly keep up with the household´s power balance at any instant of time, resulting in a mismatch between the expected and measured battery behavior under dynamic conditions. This temporal mismatch is compensated by power fed into or imported from the grid in households equipped with AC-coupled PV-battery systems. Due to the unidirectional path of DC-coupled PV-battery systems, the mismatch solely causes a grid injection and no power flow from the grid into the battery systems. They also cause additional grid supply of the load when reacting to increasing loads with a delayed response time.

The response time-induced mismatch of a PV-battery system is caused by several factors. On the one hand, the power measurements cannot be obtained in real-time without any time delay. In particular, the acquisition of measurements on the basis of counting pulses of energy meters with so-called S0 interfaces causes substantial discrepancies of up to several seconds between the actual and measured values [11]. However, more sophisticated energy metering concepts based on Modbus or CAN-bus communication protocols can provide power measurements with temporal resolutions in the range of 1 s [12,13]. Apart from the data acquisition, also the signal processing in the control unit and inverter incorporate time delays. Furthermore, an additional dead-band might be implemented in the control scheme, which further increases the response time. Moreover, for reasons of control stability, a slow reacting response of the battery system can be advantageous [14]. As a result, different elements contribute to the overall response behavior of a battery system, which is in the time-scale of up to several seconds.

There are numerous studies analyzing the benefit of combining residential PV systems with a battery storage device by simulations with temporal resolutions of 1 min or lower [15–18]. In this way, these studies do not take short-term issues, and thus the control response into account. Only a few studies carried out simulations with a time scale of less than 1 min [19,20]. Braun et al. [19] investigated the sampling interval of the energy management and their influence on the losses in self-consumed PV energy based on 1-s resolved simulations. They found out that the PV self-consumption will be reduced by around 5%, if the sampling interval is increased from 1 to 10 s. Schmiegel et al. [21] found that the reaction time of the inverter should be below 1 s to avoid significant mismatch losses. Weniger et al. [20] analyzed the impact of the response time varying from 1 to 10 s on the annual energy exchange between the household and the grid. It is shown that the amount of energy exchanged between the battery and the grid increases with a slower response time. A further study on the influence of the data acquisition response on the mismatch errors was conducted by Kreutzer et al. [13]. The investigation shows annual mismatch errors of up to 216 kWh derived from 1-s resolved load and PV output measurements from a period of 4 days. The same measurements are also integrated into the test procedure that intends to determine the dynamic performance of home-scale PV-battery systems proposed by Niedermeyer et al. [22]. Kairies et al. [23] performed measurements analyzing the response behavior of four different PV-battery systems. The authors ascertained dead

times ranging from less than 1 s to about 13 s from the experimental results. In total, the systems under study require up to 50 s to reach the steady state after a sudden load variation.

Due to the limited availability of 1-s resolved load and PV generation data, there is a significant lack of studies analyzing the impact of the response time-induced mismatch losses of residential PV-battery systems on the annual operational performance. Thus, the purpose of this paper is to examine the response behavior of such systems by means of theoretical, experimental and simulation-based investigations. The paper is organized as follows: Section 2 presents a brief theoretical investigation of the response time problem. In Section 3, high-resolution measurements taken from two different PV-battery systems are analyzed. Thereafter, Section 4 introduces the input data and applied modeling approach of the simulation study, while the simulation results of the parametric analysis are presented in Section 5. Finally, the findings are discussed and concluded in Section 6.

2 Theoretical investigation

In this section, a brief theoretical analysis of the response time issue, studying the power flows of buildings equipped with PV-battery systems, is provided. The findings are derived from a hypothetical case with and without a response time. The power flows are analyzed for AC-coupled PV-battery systems.

2.1 Power flows of PV-battery systems without any time delay

The power flows of a building equipped with a PV-battery system neglecting any response time are illustrated in Figure 1 (a). The PV generated power is primarily used to cover the local demand concurrently, indicated by the yellow arrow. The load which is directly supplied by the PV system $P_{PVS2L}(t)$ at an instant t is given by:

$$P_{PVS2L}(t) = \min(P_{PVS}(t), P_L(t)) \tag{1}$$

where $P_{PVS}(t)$ is the power output of the PV system and $P_L(t)$ the electrical load demand. The difference between the former and the latter quantity is defined as the residual power $P_R(t)$ in this study:

$$P_R(t) = P_{PVS}(t) - P_L(t) \tag{2}$$

Positive values of the residual power correspond to the residual PV power $P_{RPVS}(t) = \max(P_R(t), 0)$, while negative values indicate the residual load demand $P_{RL}(t) = \min(P_R(t), 0)$. The residual power can be regarded as the request to which the battery system must respond [24]. The resulting AC-power of the battery system is restricted by the rated AC-charging power $P_{AC2BS,MAX}$ and the rated AC-discharging power $P_{BS2AC,MAX}$. In the absence of any response time, the AC-charging power of the battery system $P_{AC2BS}(t)$, which is equal to the AC-charging power covered by the PV system $P_{PVS2BS}(t)$, is obtained by:

$$P_{AC2BS}(t) = P_{PVS2BS}(t) = \min(P_{RPVS}(t), P_{AC2BS,MAX}) \text{ if } SOC(t) < SOC_{MAX} \quad (3)$$

while the battery´s state of charge $SOC(t)$ is lower than its maximum value SOC_{MAX}. Similarly, the AC-power discharged from the battery system $P_{BS2AC}(t)$ is completely used to supply the load $P_{BS2L}(t)$ and is given by:

$$P_{BS2AC}(t) = P_{BS2L}(t) = \max(P_{RL}(t), P_{BS2AC,MAX}) \text{ if } SOC(t) > SOC_{MIN} \quad (4)$$

in cases in which the battery is not fully discharged.
The total AC-power of the battery system $P_{BS}(t)$ corresponds to the sum of the charging power $P_{AC2BS}(t)$ and discharging power $P_{BS2AC}(t)$:

$$P_{BS}(t) = P_{AC2BS}(t) + P_{BS2AC}(t) \quad (5)$$

Notice that the battery discharging power $P_{BS2AC}(t)$ has a negative sign in this definition. If the battery is empty or fully charged, the residual power will be imported from or exported to the electricity grid, respectively. The resulting power exchanged with the electricity grid can be deduced from the aforementioned quantities. The AC-power fed into the grid $P_{AC2G}(t)$ corresponds to the PV feed-in power $P_{PVS2G}(t)$ and is achieved by:

$$P_{AC2G}(t) = P_{PVS2G}(t) = P_{RPVS}(t) - P_{PVS2BS}(t) \quad (6)$$

The power supplied by the grid $P_{G2AC}(t)$ is equal to the grid supply of the load $P_{G2L}(t)$ and is calculated according to:

$$P_{G2AC}(t) = P_{G2L}(t) = P_{RL}(t) - P_{BS2L}(t) \quad (7)$$

As a result, the power exchanged with the grid $P_G(t)$ can be written as:

$$P_G(t) = P_{AC2G}(t) + P_{G2AC}(t) \quad (8)$$

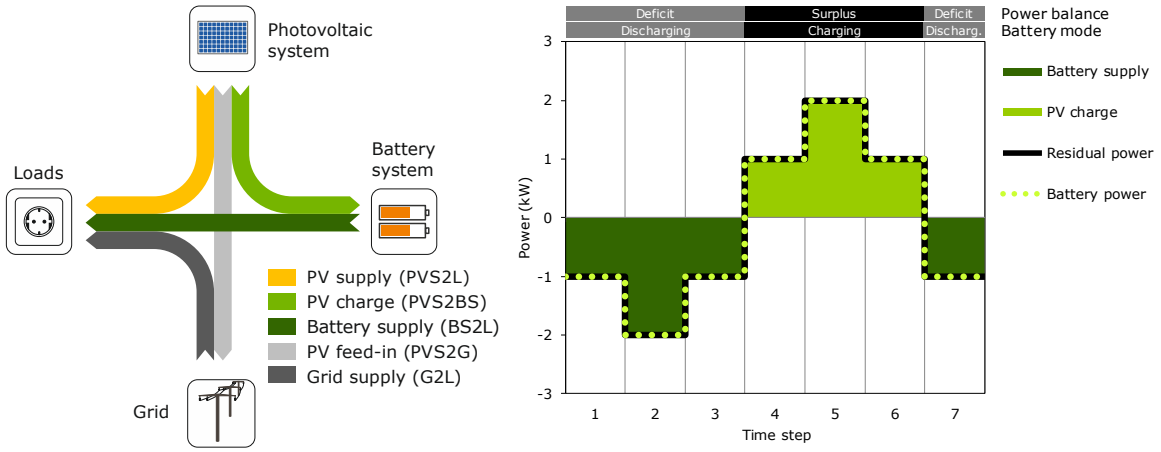

Figure 1 (a) Possible power flows of a household equipped with an AC-coupled PV-battery system in the absence of any control response time; (b) hypothetical case of the residual power and resulting battery power during seven time-steps without any response time of the battery system (assumption: the battery is neither fully charged nor completely discharged).

To demonstrate the temporal course of the power flows in the absence of any response time, Figure 1 (b) illustrates an exemplary trajectory of the residual power over a period of seven time steps. During each time step, the respective levels of the residual power are assumed to be constant. Furthermore, it is assumed that the battery is neither full nor empty. This hypothetical case includes a sequence of several ascending and descending residual power steps. The black solid line represents the resulting residual power. At every point in time, the battery power (green dotted line) matches the residual power exactly. In this way, the bright green area marks the PV energy used to charge the battery while the dark green area corresponds to the energy provided by the battery system to supply the load. The charging and discharging process correlates perfectly with the power balance within the building, as displayed in the upper part of Figure 1 (b). As a result, the battery may respond to any rapid power changes immediately in the ideal case with an instantaneous response of the battery system.

2.2 Power flows of PV-battery systems taking the time delay into account

Given the fact that the battery system cannot follow the PV output and electrical demand curves instantaneously, a temporal mismatch between the battery power and the residual power is inevitable. This discrepancy leads to an additional power exchange between the battery system and the grid, as illustrated in Figure 2 (a) with the orange- and red-colored areas. For a better understanding of the response-induced power flows, the mismatch between the residual and battery power curve is examined based on Figure 2 (b). The profile of the residual power is the same as in the example analyzed above. However, in this hypothetical case a dead time with the size of one time step is assumed. Consequently, the battery power responds to the residual power of the previous time step. The response-induced mismatch causes distinct deficit and surplus circumstances which are compensated by power absorbed from or provided by the grid.

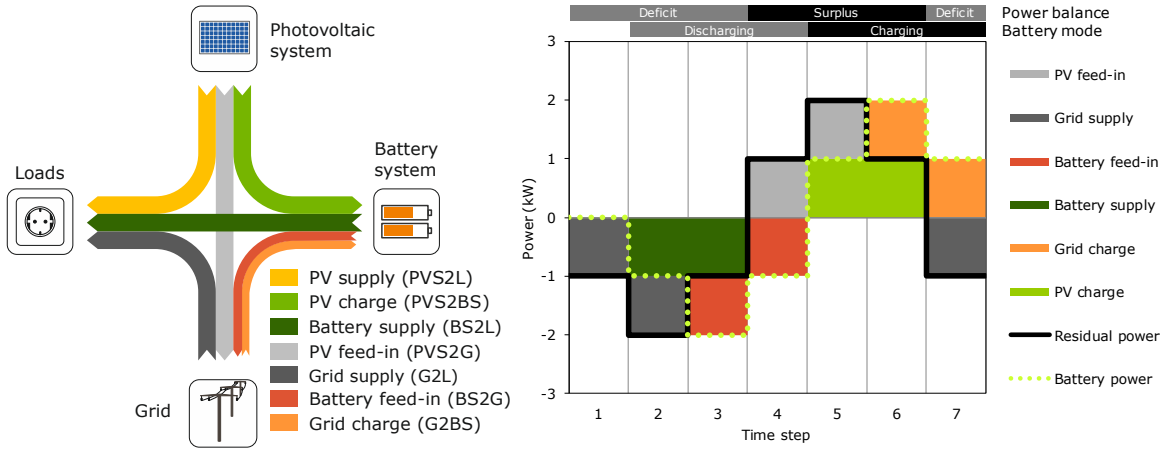

Figure 2 (a) Possible power flows of a household equipped with an AC-coupled PV-battery system under consideration of the control response time; (b) hypothetical case of the residual power and the power of the battery system during seven time-steps with an imposed dead time of one time-step.

The resulting mismatch can also be deduced from the distinct modes of the battery operation and on-site power balance, as depicted on top of the graph. By comparing the curves of the battery power and residual power, it can be seen that both curves partially overlap. At time step one; the total residual load demand is covered by power drawn from the grid. The power imported from the grid to supply the load $P_{G2L}(t)$ can be formulated as:

$$P_{G2L}(t) = \min(P_{RL}(t) - P_{BS2AC}(t), 0) \tag{9}$$

At the second step, the residual power drops to -2 kW. However, the battery discharging power is adjusted according to the previous value, due to the assumed dead time of one time step. Thereby, the load demand is only partially covered by the power discharged from the battery system $P_{BS2L}(t)$:

$$P_{BS2L}(t) = \max(P_{RL}(t), P_{BS2AC}(t)) \tag{10}$$

The discrepancy between the residual load demand and the discharging power is compensated by power imported from the grid according to Equation (9).
The subsequent positive step change in the residual power leads to the case in which the battery discharging power surpasses the residual load demand. This implies that the increased discharging power is injected into the grid $P_{BS2G}(t)$:

$$P_{BS2G}(t) = \min(P_{BS2AC}(t) - P_{RL}(t), 0) \tag{11}$$

At time step four, the residual power is already positive while the battery power is still negative. Such circumstances are caused by a change from a deficit to a surplus power balance. Consequently, both the battery power and the residual PV power are injected into the grid. The grid feed-in power of the PV system $P_{PVS2G}(t)$ is obtained by:

$$P_{PVS2G}(t) = \max(P_{RPVS}(t) - P_{AC2BS}(t), 0) \quad (12)$$

In the next time step, the battery charging power covered by the residual PV power $P_{PVS2BS}(t)$ is given by:

$$P_{PVS2BS}(t) = \min(P_{RPVS}(t), P_{AC2BS}(t)) \quad (13)$$

As defined in Equation (12), the remaining PV surplus will be injected into the grid. At time step six, the available residual PV power falls below the battery charging power so that the power used to charge the battery is partially covered by power drawn from the grid $P_{G2BS}(t)$:

$$P_{G2BS}(t) = \max(P_{AC2BS}(t) - P_{RPVS}(t), 0) \quad (14)$$

Another distinct event appears in the last time step. Meanwhile, the residual power becomes negative whereas the battery charging persists. Therefore, the battery charging power as well as the residual load demand are supplied by the grid. Both quantities can be extracted from Equation (9) and (14). Although this specific example is of theoretical nature, all relevant power flows induced by the response behavior can be deduced from it. Therefore, this hypothetical case enables to understand the effects of the response time on the power flows occurring in grid-tied households equipped with AC-coupled PV-battery systems.

3 Experimental investigation

In this experimental section, the presence of the delayed response behavior of PV-battery systems should be demonstrated based on experimental data obtained from a measurement campaign. The measurements were taken in two detached houses equipped with different grid-connected PV-battery systems. The characteristics of the investigated PV-battery systems are summarized in Table I. All the systems under study are equipped with a lithium-ion battery and a single-phase battery inverter. The Sonnenbatterie Comfort S is an AC-coupled PV-battery system with 5.7 kWh of usable battery capacity. The E3DC S10-E5 system is DC-coupled with 5.4 kWh of usable battery capacity.

Table I Characteristics of the PV-battery systems under study.

Manufacturer	Model	Battery capacity	System topology	Year of installation
Sonnenbatterie	Comfort S	5.7 kWh	AC-coupled	2013
E3DC	S10-E5	5.4 kWh	DC-coupled	2013

3.1 Test setup and procedure

The power flows within the residual buildings were recorded temporarily using two mobile measuring devices with a temporal resolution in the order of 0.25 s. Both measuring instruments are identical and equipped with a WAGO 750-494 three-phase power measurement module. In order to assess the response behavior of the battery systems, the residual power as well as the battery power have to be measured. A schematic representation of the measurement setup and the location of the power measurements within the household's AC-bus are shown in Figure 3. Due to the local circumstances, it was not possible to measure the battery power in the house in which the Sonnenbatterie system is installed. Thereby, the dynamic performance of the Sonnenbatterie was determined indirectly by measuring the residual power $P_R(t)$ and the power exchanged with the grid $P_G(t)$. In this way, the battery power $P_{BS}(t)$ can be calculated via:

$$P_{BS}(t) = P_R(t) - P_G(t) \tag{15}$$

The electrical wiring within the building equipped with the E3DC battery system does not allow to measure the residual power; hence the residual power was determined by means of measuring the battery and grid power according to Equation (15).

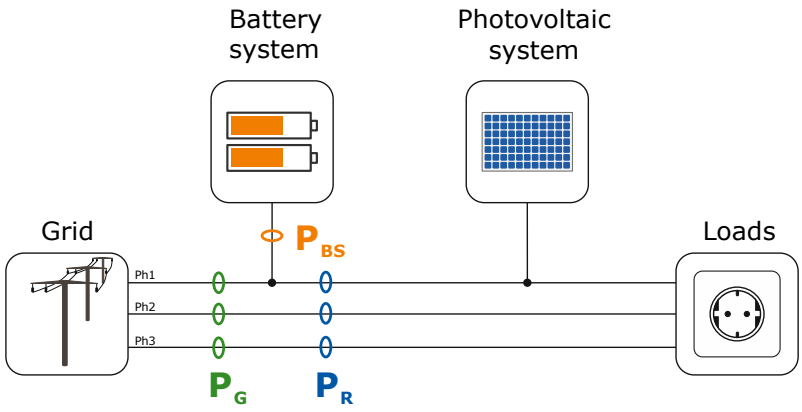

Figure 3 Measurement points of the different quantities to determine the response behavior of AC-coupled PV-battery systems (P_{BS} battery power; P_G grid power; P_R residual power). At least two of the three power flows have to be measured.

To analyze the mismatch between the residual power and the measured power of the battery systems under study, an on-site step response experiment was conducted. A cooking plate with 1.5 kW of nominal power served as a controllable load. The measurements were taken over of a period of 60 s under real operational conditions. The step load profile was created by switching the load on and off after 10 s and 40 s, respectively. To prevent additional fluctuations in the residual power during the experiment, the measurements were carried out during times with steady-state electrical load demand and no PV power output. Therefore, the modulus of the residual power is equal to the total power consumed by the electrical devices and controllable load during the measurement period.

It should be mentioned that the internal timing of the two measuring devices do not match exactly, and therefore, differences in the time step intervals of the two measured quantities occur. Thereby, a post-processing procedure was applied to synchronize the timing of the measured time series. As the time stamps are not equidistant, the time stamp mismatching in the time scale of 0.1 s cannot completely be eliminated. For a better comparability between the measurements in the different buildings, the remaining on-site load demand was subtracted from the measured power flows. This eliminated offset varies between 360 W and 370 W during the survey of the two systems. For this reason, it can be summarized that the dynamic behavior of the battery systems was measured under almost identical conditions.

3.2 Experimental results

The measured response of the two PV-battery systems is analyzed in this section. Figure 4 (a) shows the response of the E3DC S10-E5 obtained from the measurements over period of 60 s. Within the first 10 s of the experiment, both the residual and the battery power are in a steady-state condition. An abrupt drop in the residual power after switching the controllable load on can be observed after 10 s. The E3DC S10-E5 follows the load change after an initial dead time of about 1 s with a steep slope of the battery power. The system takes additional 1.5 s to reach the steady state for the first time. Subsequently, a small undershoot can be noticed. In total, the E3DC S10-E5 battery system settles to the new stationary conditions within about 5 s. After 40 s, the battery system is subjected to a positive step change induced by switching off the controllable load. The subsequent response behavior is almost identical to the one observed after the negative step change. The E3DC S10-E5 takes a total of approximately 5 s to reach a steady state, which is comparable to the settling time after the abrupt decrease in the residual power.

The experimental results acquired from measurements of the Sonnenbatterie Comfort S are displayed in Figure 4 (b). As the step changes are obtained by switching the controllable load manually, both residual power profiles differ slightly from each other. The Sonnenbatterie responds to the step changes after about 1.5 s. However, differences in the response behavior depending on whether the residual power decreases or rises can be observed. By comparing both graphs in Figure 4, it can clearly be seen that both systems have different response behaviors with distinct time constants. The Sonnenbatterie Comfort S reaches the steady state after a drop and increase in the residual power within about 7 and 5 s, respectively. As the settling time may vary depending on the instant in time the load step is applied and the magnitude of the load step (cf. [23,25]), no general conclusions about the dynamic response of both systems should be drawn from this single experiment. In addition, for reasons of reproducibility, the test-procedure was only performed during the discharge process. In this way, the dynamic response during the charging process of the battery systems could not be deduced from the measurements. Nevertheless, first insights of the response behavior can be concluded from them.

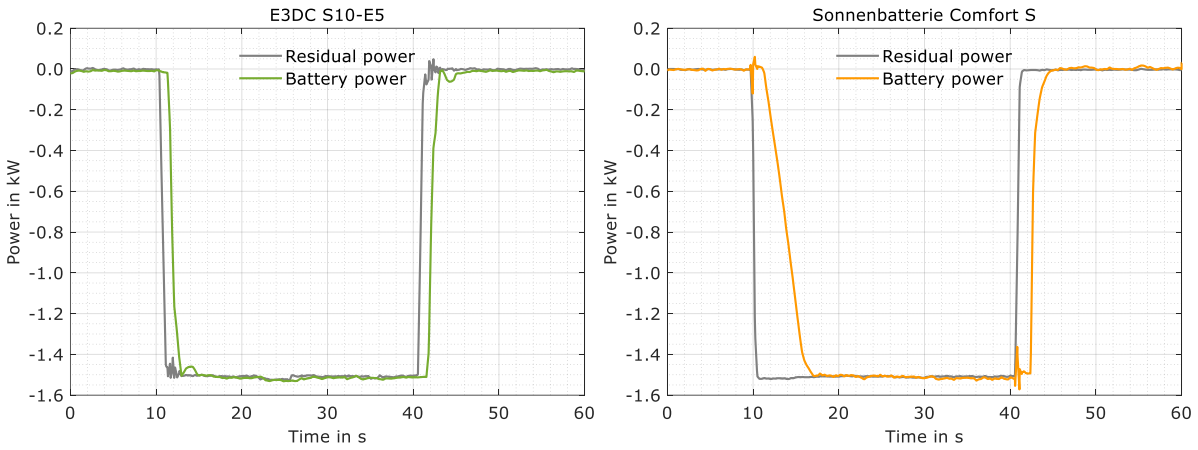

Figure 4 Measured dynamic response of the E3DC S10-E5 (a) and Sonnenbatterie Comfort S (b) during a step response experiment.

4 Methods of the simulation study

To get a more holistic view on the response time topic, a simulation study analyzing the annual mismatch losses is carried out. In this section, an overview of the applied models and used input data is provided. The simulations are carried out in the MATLAB environment with a temporal resolution of one second over a simulation period of one year.

4.1 High-resolution weather and load data

Firstly, the PV system's power output is calculated based on meteorological measurements performed by the University of Oldenburg, Germany [26]. The chosen data set includes measured values of the air temperature as well as diffuse and global irradiance taken every second from January to December 2014. The measurements of the temperature and irradiance quantities are captured by Pt-100 temperature sensors and Kipp & Zonen CM11 pyranometers, respectively. During the period under study, the global irradiation on the horizontal plane amounts to 1065 kWh/m².
Secondly, a load data set provided by the Institute for Future Energy Systems (IZES) serves as an input for the electricity consumption [27]. Therein, time series of the load demand of various households with a temporal resolution of 15 min are included. In this study, the load profile of one household with an annual load demand of 5 MWh is used for the calculations. To increase the temporal resolution of the load profile from 15 min to 1 s, an additional load profile synthesis was applied [28]. The 1-s resolved load profile is synthesized out of load measurements from 30 Austrian households provided by the Vienna University of Technology (TU Wien) [29]. Each 15-min time frame of the load profile under consideration is substituted by a 1-s resolved time series with the same amount of energy. As a result, the synthetically generated load profile preserves the primary course of the 15-min resolved load profile while the distinctive short-term load fluctuations occurring in several households are added. Further details concerning the load profile synthesis used in this paper can be found in [28].

4.2 PV-battery system model

Based on the horizontal irradiance measurements, the irradiance on the plane of the PV array is calculated by means of geometric relations and the Klucher model [30]. The PV generator is oriented with a 35° tilt angle due south and is modelled using an empirical model [31]. Therein, the PV module efficiency is calculated as a function of the irradiance on the plane of array and the air temperature. In addition, distinct generator losses are depicted by empirical factors [32]. Then, the efficiency of the PV inverter is modelled alike [33]. The maximum inverter power is set to 1 kW/kWp and the resulting specific power output of the PV system is scaled to a rated PV power of 5 kWp.

Both the time series of the PV power output as well as the synthetically generated load profile are the basis for simulating the charging and discharging behavior of the battery system. To simply incorporate the observed dynamic behavior of the battery systems in the simulations, a first-order time delay element (low-pass filter) is implemented in the battery control unit. In this way, the response of the battery power $P_{BS}(t)$ on the residual power $P_R(t)$ is obtained as:

$$P_{BS}(t) = \begin{cases} P_{BS}(t - \Delta t) + (P_R(t - t_{DT}) - P_{BS}(t - \Delta t)) \cdot \left(1 - e^{-\frac{\Delta t}{\tau}}\right) \text{ if } \tau > 0\ \text{s} \\ P_R(t - t_{DT}) \text{ if } \tau = 0\ \text{s} \end{cases} \quad (16)$$

where t_{DT} is the dead time, Δt the time step size and τ the time constant. The response behavior is assumed to be identical during the charging and discharging processes.

For simplicity, the efficiency of the AC-coupled lithium-ion battery storage system is modeled by constant efficiency factors [4]. The losses of the battery converter are considered with a constant efficiency factor of 94%. The watt-hour efficiency of the battery is set to 95%. Moreover, the maximum battery power is limited to 1 kW/kWh and the usable battery capacity is set to 5 kWh. The battery system´s mode of operation is aimed at maximizing the on-site self-sufficiency, and thereby the battery is charged with the first available residual PV power.

5 Simulation results and sensitivity analysis

This section presents the results of the simulation study, which is based on the described input data and models. The additional annual amount of energy exchanged with the grid due to the control response is analyzed. By varying the dead time and time constant (Figure 5), the impact of both variables is studied. The analysis is also conducted for a variety of system sizes in terms of rated PV power and usable battery capacity.

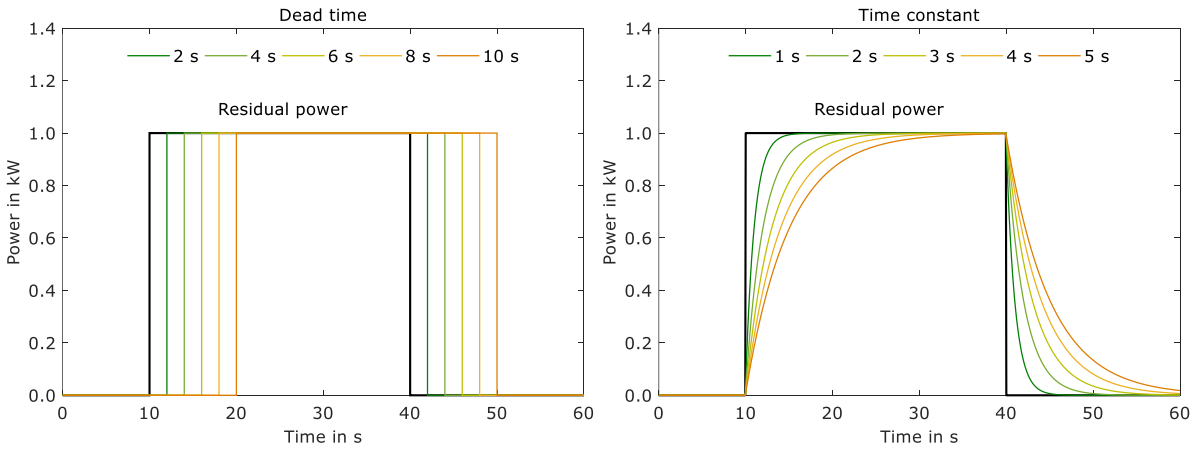

Figure 5 Modelled dynamic response of an AC-coupled PV-battery system with various dead times (a) and various time constants (b).

5.1 Varying dead time

The response behavior of battery systems is accompanied by a time lag, as shown in Section 3. To gain a better understanding of the resulting energy flows caused by the time delay, the impact of the dead time is analyzed without a time constant in this subsection. Figure 6 (a) shows the residual PV power and battery power over a period of 5 min, in which the variability of the excess PV power is mainly caused by passing clouds. The battery system reacts to the residual power with an assumed time delay of 5 s. By doing so, the battery profile (green line) and the residual power profile (black line) are only partially overlapped. As already stated above, this leads to an increase in the power exchanged with the grid. During events with steep increases in the residual PV power, an additional PV feed-in (grey area) can be observed. After the decrease in the residual PV power, the increased battery power is compensated by absorbing the additional power from the grid (orange area).

The impact of the dead time on the power flows can also be observed during the discharging process, as shown in Figure 6 (b). During the exemplary time frame of 5 min, distinct fluctuations appear in the residual power profile due to switching electrical devices. The temporal mismatch between the battery power and residual load demand induced by the dead time of 5 s can be noticed especially after sudden load variations. As a result of a drop in the residual power, i.e. increase in the load demand, the residual power falls below the battery power and the difference is supplied by the grid. Once an increase in the residual power occurs, the surplus battery power is injected into the grid. Electrical appliances with rectangle-shaped demand curves can cause situations in which the battery is discharged asynchronously to the load demand, depending on the time lag of the system control and the frequency of the load fluctuations. Consequently, sudden short load peaks, e.g. caused by electric cooking plates, cannot be completely covered by power discharged from the battery system due to its inherent dead time.

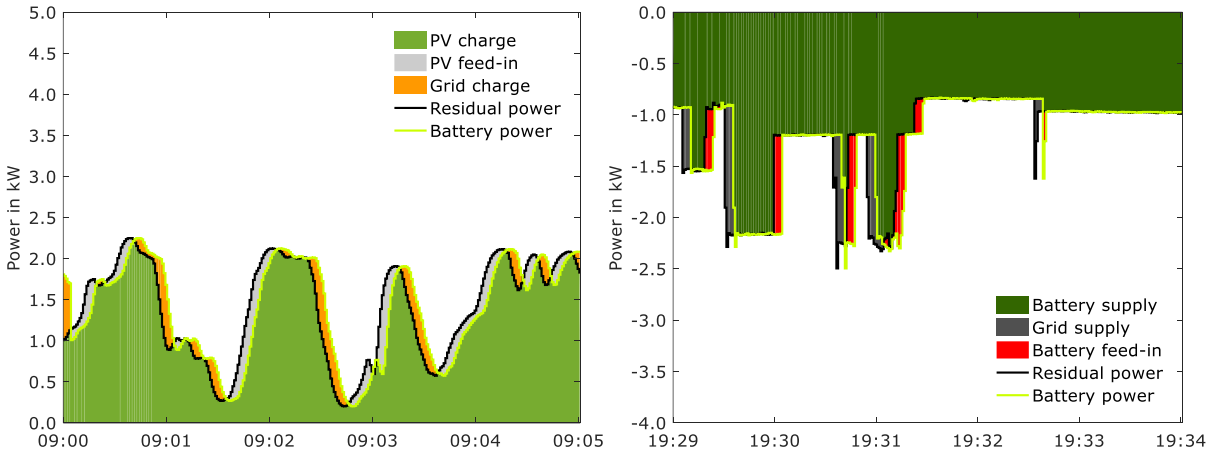

Figure 6 Power flows within two exemplary time frames during the charging process (a) and discharging process (b) taking a dead time of 5 s into account.

To quantify the dead time-induced increase in the annual grid feed-in and grid supply, simulations using dead times ranging from 1 to 10 s were carried out over period of one year. For the reference case without any control response, the annual energy drawn from the grid amounts to 2238 kWh/a and the annual energy fed into the grid amounts to 2059 kWh/a. As might be expected, an increasing dead time is associated with an increase in the energy amount exchanged with the grid; hence the longer the dead time, the larger the grid feed-in and the larger the grid supply. By comparing Figure 7 (a) and (b), it can be noticed that the increase in the grid feed-in is equal to the increase in the grid supply. This may be explained by the fact that the dead time-induced non-overlapping areas under the curves are of the same size for the feed-in and grid supply over a period of one year.

A dead time of 5 s results in an increase in the annual energy exchanged with the grid of 90 kWh/a compared with the ideal case without any time delay. If the battery system responds with a delay of 10 s, the exchanged energy is increased to about 140 kWh/a. As such, a nonlinear relationship between the mismatched amount of energy and the dead time is visible, which has already been found by Braun et al. [19]. Moreover, the increase in the grid feed-in is mainly caused by the battery feed-in while the increase in the energy drawn from the grid mainly supplies the load. It can be highlighted that the influence of the dead time on the additional PV feed-in is much lower compared to the battery feed-in. The results also show that the increase in the battery feed-in is equal to the increase in the grid supply of the loads. Consequently, more energy is fed into the grid from the battery system than is absorbed from the grid by the battery. As the discharge process is mainly affected by the load curve, this fact reveals that the mismatch due to the dead time is greatly attributable to load fluctuations. Moreover, the total operating time of the battery system during discharging is higher than it is during charging.

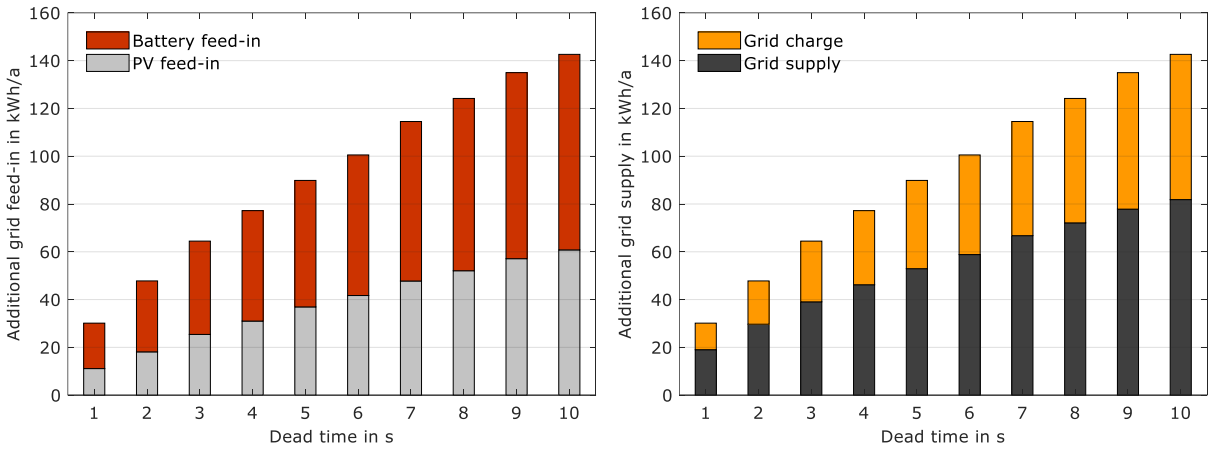

Figure 7 Annual increase in the grid feed-in (a) and grid supply (b) as a function of the dead time compared to the reference case without a time constant.

5.2 Varying time constant

In the following, it is analyzed how the time constant of the first-order time delay element affects the power flows and the annual amount of energy exchanged with the grid. For the sole purpose of identifying the impact of the time constant, no dead time is considered. Figure 8 (a) illustrates the dynamic response when a time constant of 2.5 s is applied. Compared to the battery power profile obtained by applying a dead time, an additional time constant smooths out the variability of the battery power profile. As a result, the course of the battery power differs from the course of the residual power and the battery power changes more slowly in cases in which the available residual PV power drops or rises abruptly. This implies a time constant-induced mismatch, which is balanced by the grid similarly to the one caused by the dead time. Figure 8 (b) shows how the time constant of 2.5 s influences the power flows during the discharge process. When the power balance suddenly changes, the battery power needs several seconds to reach the steady state. As can be seen, the greater the drop or rise in the residual power, the larger the amount of energy exchanged with the grid.

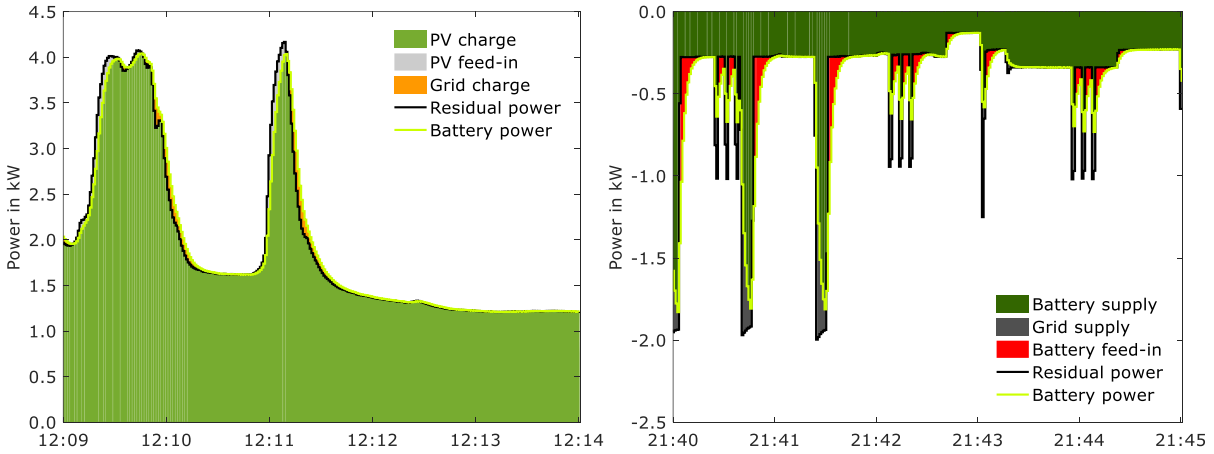

Figure 8 Power flows within two exemplary time frames during the charging process (a) and discharging process (b) taking a time constant of 2.5 s into account.

Moreover, yearly simulations were carried out with different time constants ranging from 0.5 to 5 s. The annual increase in the energy absorbed from or injected to the grid was calculated based on the simulation results, as displayed in Figure 9. Similar to the results obtained for varying dead times, an increasing time constant leads to an increase in the energy exchanged with the grid. By applying a time constant of 2.5 s, the grid feed-in as well as the grid supply are increased by roughly 37 kWh/a. A time constant of 5 s results in an increased amount of energy of 65 kWh/a exchanged with the grid. A comparison of both graphs shows that the battery feed-in is smaller compared to the increase in the grid supply to cover the loads. This can be explained with the circumstance that the magnitude of the negative ramps of the residual load differs from the magnitude of the positive ramps of the residual load during the discharge process.

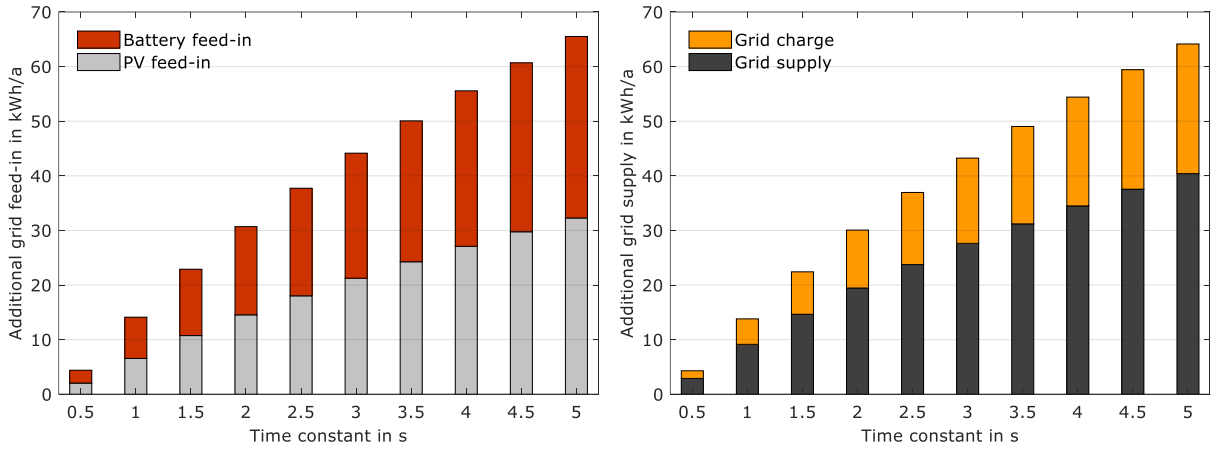

Figure 9 Annual increase in the grid feed-in (a) and grid supply (b) as a function of the time constant compared to the reference case without a dead time and without a time constant.

5.3 Varying dead time and time constant

In this subsection, the impact of the dead time as well as the time constant is investigated. This is realized by applying both a dead time and a time constant in the control scheme. Figure 10 shows the simulation results and the increase in the amount of energy exported to the grid (a) and imported from the grid (b). Without a time constant, the results for the grid feed-in and grid supply are similar to the one presented in Figure 7. In the absence of the dead time, the amount of energy exchanged with the grid is increased by about 65 kWh/a for a time constant of 5 s (cf. Figure 9). Nevertheless, the time constant-induced increase in the energy exchanged with the grid tends to decrease with an increasing dead time. If the dead time is set to 10 s, an additional time constant of 5 s will only increase the energy exchanged with the grid by about 20 kWh/a. This is due to the time constant caused smoothing during the charging and discharging of the battery system. It can be concluded that the energy exchanged with the grid is affected by the dead time more than it is by the time constant.

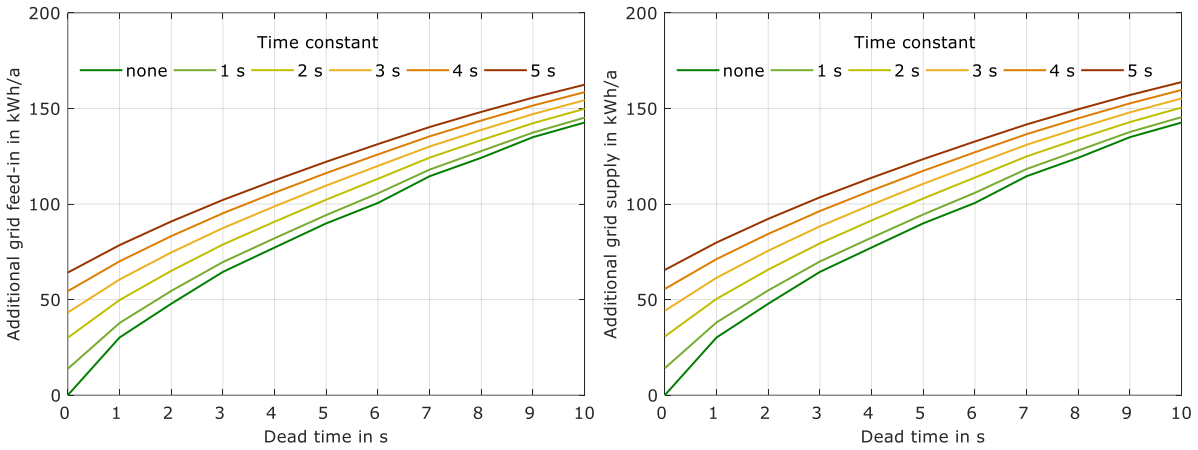

Figure 10 Annual increase in the grid feed-in (a) and grid supply (b) as a function of the time constant and dead time compared to the reference case without a dead time and without a time constant.

5.4 Varying size of the PV system and battery storage

As the simulation results presented above are obtained for a PV-battery system with 5 kWp of installed PV power and 5 kWh of usable battery capacity, a sensitivity analysis was performed by varying both parameters to identify the impact of the system size. For reason of comparability, the rated PV inverter power and the rated battery power were also scaled with the size of the PV-battery system (c.f. Section 4.2). A dead time of 5 s without a time constant was taken as the reference for the sensitivity analysis.

Figure 11 (a) presents the additional amount of energy imported from the grid as a function of the system configuration in terms of rated PV power and battery capacity. As was demonstrated in Section 5.1, the increase in the grid supply is identical to the increase in the grid feed-in as long as the battery system reacts to power fluctuations with only a dead time and no time constant. Analyzing Figure 11 (a), it is obvious that the increase in the grid supply depends on the relationship between the storage capacity and rated PV power. In general, as the battery capacity increases, the dead time-induced additional grid supply also increases. This is mainly due to the fact that the dwell time in the charge and discharge mode increases with the battery size.

By solely enlarging the PV system size, the additional amount of energy imported from the grid rises first. However, with a larger PV system, the energy exchanged with the grid falls or remains unchanged. This can be explained as follows: With an increasing PV system size, the battery discharging will be shifted more and more from times in the afternoon or evening to night-time with a less fluctuating load demand. The dead time under study results in an increase of the annual grid supply of 90 kWh/a for a PV-battery system with 5 kWp of installed PV power and 5 kWh of usable battery capacity (cf. Figure 7). If the system configuration is twice as large, the increase in the grid supply amounts to approximately 120 kWh/a.

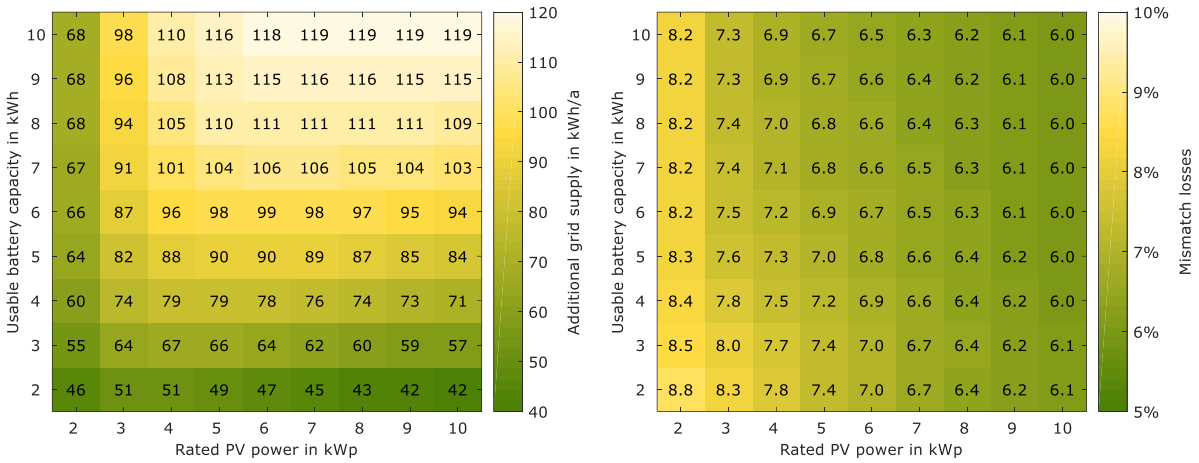

Figure 11 Impact of the system configuration in terms of rated PV power and usable battery capacity on the annual increase of the grid supply (a) and control response-induced mismatch losses (b) for a dead time of 5 s.

When comparing the absolute increase of the grid supply of different system configurations, the varying energy throughput of the battery system must be considered. To ensure better comparability, it is beneficial to consider the additional increase of the grid supply ΔE_{G2AC} in relation to the amount of energy discharged from the battery system E_{BS2AC}. The control response time-induced mismatch losses m can be obtained as:

$$m = \frac{\Delta E_{\mathrm{G2AC}}}{E_{\mathrm{BS2AC}}} \tag{17}$$

The mismatch losses also represent the ratio between the additional grid supply and the theoretically avoidable grid supply, which is equal to the amount of energy discharged from the battery system. Thereby, this assessment criterion enables drawing conclusions on how effectively the battery system can be used to reduce the grid supply. Figure 11 (b) illustrates the annual mean of the calculated mismatch losses for different system configurations. It is clearly visible that the highest control response-induced mismatch-losses are obtained for small-sized PV-battery systems. When combining 2 kWh of usable battery capacity and 2 kWp of rated PV power, the mismatch losses induced by 5 s of dead time amount to 8.8%. Increasing the size of the PV system and storage device will decrease the mismatch losses. As the simulation results reveal, the mismatch losses amount to 6% for the largest system configuration under study. From an energetic point of view, the mismatch losses considerably affect the household´s energy balance.

6 Conclusions

In this paper, the dynamic performance of PV-battery systems with respect to the capability to follow residual power fluctuations was assessed. Firstly, the response time issue was analyzed from a theoretical perspective. It was revealed how the resulting mismatch affects the energy flows between the household and the grid. Moreover, the matching accuracy of two PV-battery systems was investigated in a step-response experiment during the discharge process. Settling times of up to 7 s to reach the steady

state after a load step of 1.5 kW were derived from the measurements. Through a simulation study the impact of the dead time and the impact of the time constant were identified and the additional annual amount of energy exchanged with the grid was determined. The longer the response time, the larger the grid feed-in and the larger the grid supply. For a typical PV-battery system with 5 kWp of rated PV power and 5 kWh of usable capacity, a dead time of 5 s increases the annual grid feed-in and grid supply by about 90 kWh/a. From an economical point of view of a German system owner, the additional feed-in is valued at 0.12 €/kWh and the additional grid supply is valued at about 0.28 €/kWh at present. As a consequence, the larger feed-in revenues (11 €/a) partially compensate the increase in costs for the energy supplied by the grid (25 €/a). The resulting net financial loss for the system owner in this example with a dead time of 5 s amounts to 14 €/a. Therefore, it can be summarized that slow-reacting battery systems are disadvantageous for the system owner.

The results obtained in this paper suggest that more in-depth experimental and simulation analyses should be addressed in further research. On the one hand, the sensitivity of the response time regarding the magnitude of the load step should be studied in detail. On the other hand, the impact of the shape and short-term variability of the load profile on the calculated annual energy balance must be evaluated. In addition, the response time issue of the battery systems should also be assessed from the grid operator´s point of view. This study also underscores the need to develop standardized test procedures to assess the dynamic performance of grid-connected PV-battery systems. To improve comparability between the different products from the end-customer´s point of view, response time-related specifications should be stated in the data sheets in the future.

Acknowledgements

The authors thank the German Federal Ministry of Economics and Technology (BMWi) and the Projektträger Jülich (PtJ) for the support of the project “LAURA” (grant number 0325716G).

References

[1] C. Breyer, A. Gerlach, Global overview on grid-parity, Prog. Photovolt. Res. Appl. 21 (2013) 121–136. doi:10.1002/pip.1254.

[2] J. Weniger, J. Bergner, T. Tjaden, V. Quaschning, Economics of residential PV battery systems in the self-consumption age, in: 29th Eur. Photovolt. Sol. Energy Conf. Exhib., Amsterdam, 2014. doi:10.4229/EUPVSEC20142014-7DO.14.3.

[3] R. Luthander, J. Widén, D. Nilsson, J. Palm, Photovoltaic self-consumption in buildings: A review, Appl. Energy. 142 (2015) 80–94. doi:10.1016/j.apenergy.2014.12.028.

[4] J. Weniger, T. Tjaden, V. Quaschning, Sizing of Residential PV Battery Systems, Energy Procedia. 46 (2014) 78–87. doi:10.1016/j.egypro.2014.01.160.

[5] J. Weniger, T. Tjaden, J. Bergner, V. Quaschning, Emerging Performance Issues of Photovoltaic Battery Systems, in: 32nd Eur. Photovolt. Sol. Energy Conf. Exhib., München, 2016: pp. 2372–2380. doi:10.4229/EUPVSEC20162016-6DP.2.1.

[6] J. Moshövel, K.-P. Kairies, D. Magnor, M. Leuthold, M. Bost, S. Gährs, E. Szczechowicz, M. Cramer, D.U. Sauer, Analysis of the maximal possible grid relief from PV-peak-power impacts by using storage systems for increased self-consumption, Appl. Energy. 137 (2015) 567–575. doi:10.1016/j.apenergy.2014.07.021.

[7] J. Li, M.A. Danzer, Optimal charge control strategies for stationary photovoltaic battery systems, J. Power Sources. 258 (2014) 365–373. doi:10.1016/j.jpowsour.2014.02.066.
[8] J. von Appen, T. Stetz, M. Braun, A. Schmiegel, Local Voltage Control Strategies for PV Storage Systems in Distribution Grids, IEEE Trans. Smart Grid. 5 (2014) 1002–1009. doi:10.1109/TSG.2013.2291116.
[9] K. Lappalainen, S. Valkealahti, Recognition and modelling of irradiance transitions caused by moving clouds, Sol. Energy. 112 (2015) 55–67. doi:10.1016/j.solener.2014.11.018.
[10] S. Cao, K. Sirén, Impact of simulation time-resolution on the matching of PV production and household electric demand, Appl. Energy. 128 (2014) 192–208. doi:10.1016/j.apenergy.2014.04.075.
[11] SMA Solar Technology AG, ed., SMA Smart Home Planning Guidelines, (2015).
[12] J. Binder, J.C. Marcel, A. Schmiegel, U. Thomas, N. Martin, C. Jehoulet, M. Landau, H.-D. Mohring, The Sol-Ion System: Prototype Deployment in French Overseas and Southern German Field Trial Locations and Logged Parameters for PV Storage System at Home Locations, in: 26th Eur. Photovolt. Sol. Energy Conf. Exhib., Hamburg, 2011. doi:10.4229/26thEUPVSEC2011-5BV.2.3.
[13] N. Kreutzer, J. Schiel, M. Rothert, Netzgekoppelte PV-Speichersysteme: Fünf Jahre Felderfahrung und Lessons Learned, in: 30 Symp. Photovoltaische Solarenergie, Bad Staffelstein, 2015.
[14] V. Eichler, Kleinsteuerungen in solaren Energiespeichern, Etz Elektrotechnik Autom. 12/2013 (2013) 51–53.
[15] G. Mulder, F.D. Ridder, D. Six, Electricity storage for grid-connected household dwellings with PV panels, Sol. Energy. 84 (2010) 1284–1293. doi:10.1016/j.solener.2010.04.005.
[16] Braun, M., Büdenbender, K., Magnor, D., Jossen, A., Photovoltaic Self-Consumption in Germany - Using Lithium-Ion Storage to Increase Self-Consumed Photovoltaic Energy, in: 24th Eur. Photovolt. Sol. Energy Conf., Hamburg, 2009: pp. 3121–3127. doi:10.4229/24thEUPVSEC2009-4BO.11.2.
[17] J. Hoppmann, J. Volland, T.S. Schmidt, V.H. Hoffmann, The economic viability of battery storage for residential solar photovoltaic systems – A review and a simulation model, Renew. Sustain. Energy Rev. 39 (2014) 1101–1118. doi:10.1016/j.rser.2014.07.068.
[18] J. Linssen, P. Stenzel, J. Fleer, Techno-economic analysis of photovoltaic battery systems and the influence of different consumer load profiles, Appl. Energy. (2015). doi:10.1016/j.apenergy.2015.11.088.
[19] M. Braun, K. Büdenbender, M. Landau, D.U. Sauer, D. Magnor, A.U. Schmiegel, Charakterisierung von netzgekoppelten PV-Batterie-Systemen - Verfahren zur vereinfachten Bestimmung der Performance, in: 25 Symp. Photovoltaische Solarenergie, Bad Staffelstein, 2010.
[20] J. Weniger, T. Tjaden, V. Quaschning, Reaktionsvermögen von Solarstromspeichern, PV Mag. (2015) 50–52.
[21] A. Schmiegel, K. Koch, A. Meissner, P. Knaup, C. Jehoulet, H. Schuh, M. Landau, M. Braun, K. Bündenbender, R. Geipel, C. Vachette, D.U. Sauer, D. Magnor, J.C. Marcel, The Sol-Ion System, an Integrated PV-System with Lithium.Ion Batteries – System Performance, in: 25th Eur. Photovolt. Sol. Energy Conf. Exhib., Valencia, 2010. doi:10.4229/25thEUPVSEC2010-4CO.1.1.
[22] F. Niedermeyer, J. von Appen, T. Kneiske, M. Braun, A. Schmiegel, N. Kreutzer, M. Rothert, A. Reischl, Innovative Performancetests für PV-Speichersysteme zur Erhöhung der Autarkie und des Eigenverbrauchs, in: 30 Symp. Photovoltaische Solarenergie, Bad Staffelstein, 2015.
[23] K.-P. Kairies, D. Haberschusz, J. van Ouwerkerk, J. Strebel, O. Wessels, D. Magnor, J. Badeda, D.U. Sauer, Wissenschaftliches Mess- und Evaluierungsprogramm Solarstromspeicher - Jahresbericht 2016, Institut für Stromrichtertechnik und Elektronische Antriebe (ISEA), RWTH Aachen, Aachen, 2016.
[24] F. Braam, R. Hollinger, C. Lübeck, S. Müller, B. Wille-Haussmann, Grid-Oriented Operation of Photovoltaic-Battery Systems, in: Int. ETG-Kongr. 2013, ETG, Berlin, 2013.

[25] C. Messner, J. Kathan, C. Seitl, S. Hofmüller, R. Bründlinger, Efficiency and Effectiveness of PV Battery Energy Storage Systems for Residential Applications - Experience from Laboratory Tests of Commercial Products, in: 32nd Eur. Photovolt. Sol. Energy Conf. Exhib., Munich, 2016.
[26] J. Kalisch, T. Schmidt, D. Heinemann, E. Lorenz, Continuous meteorological observations in high-resolution (1Hz) at University of Oldenburg in 2014, (2015). http://dx.doi.org/10.1594/PANGAEA.847830 (accessed September 7, 2015).
[27] P. Hoffman, G. Frey, M. Friedrich, S. Kerber-Clasen, J. Marschall, M. Geiger, Praxistest „Moderne Energiesparsysteme im Haushalt“, Institut für ZukunftsEnergieSysteme, Saarbrücken, 2012.
[28] J. Weniger, J. Bergner, T. Tjaden, J. Kretzer, F. Schnorr, V. Quaschning, Einfluss verschiedener Betriebsstrategien auf die Netzeinspeisung räumlich verteilter PV-Speichersysteme, in: 30 Symp. Photovoltaische Solarenergie, Bad Staffelstein, 2015.
[29] A. Einfalt, A. Schuster, C. Leitinger, D. Tiefgraber, M. Litzlbauer, S. Ghaemi, D. Wertz, A. Frohner, C. Karner, Konzeptentwicklung für ADRES - Autonome Dezentrale Erneuerbare Energie Systeme, Wien, 2012.
[30] T.M. Klucher, Evaluation of models to predict insolation on tilted surfaces, Sol. Energy. 23 (1979) 111–114. doi:10.1016/0038-092X(79)90110-5.
[31] H.G. Beyer, G. Heilscher, S. Bofinger, Identification of a General Model for the MPP Performance of PV-Modules for the Application in a Procedure for the Performance Check of Grid Connected Systems, in: 19th Eur. Photovolt. Sol. Energy Conf., Paris, 2004: pp. 3073–3076.
[32] E. Lorenz, T. Scheidsteger, J. Hurka, D. Heinemann, C. Kurz, Regional PV power prediction for improved grid integration, Prog. Photovolt. Res. Appl. 19 (2011) 757–771. doi:10.1002/pip.1033.
[33] H. Schmidt, D.-U. Sauer, Wechselrichter-Wirkungsgrade: Praxisgerechte Modellierung und Abschätzung, Sonnenenergie. 4 (1996) 43–47.